Processing and Application of Ceramics 11 [1] (2017) 27–38
DOI: 10.2298/PAC1701027S

Enhanced photocatalytic degradation of RO16 dye using Ag modified ZnO nanopowders prepared by the solvothermal method

Bojana Simović[1,*], Dejan Poleti[2], Aleksandar Golubović[3], Aleksandar Matković[3], Maja Šćepanović[3], Biljana Babić[4], Goran Branković[1]

[1]*Institute for Multidisciplinary Research, University of Belgrade, Kneza Višeslava 1, 11030, Belgrade, Serbia*
[2]*Department of General and Inorganic Chemistry, Faculty of Technology and Metallurgy, University of Belgrade, Karnegijeva 4, 11120 Belgrade, Serbia*
[3]*Center for Solid State Physics and New Materials, Institute of Physics, University of Belgrade, Pregrevica 118, 11080 Belgrade, Serbia*
[4]*Institute of Nuclear Sciences "Vinča", University of Belgrade, 11001 Belgrade, Serbia*

Received 13 October 2016; Received in revised form 30 January 2017; Accepted 18 February 2017

Abstract

In this work, $Zn(CH_3COO)_2 \cdot 2H_2O$ with $AgNO_3$ content from 0 to 6 mol% was solvothermally treated at 120 °C for 18 h in the presence of poly(vinyl pyrrolidone), ethylene glycol and sodium hydroxide. The structural, microstructural and photocatalytic properties of the unmodified and Ag modified ZnO powders have been investigated by the XRPD, FESEM, TEM, UV-vis, Raman and BET techniques. The Ag modified samples consist of ZnO nanocrystals and metallic Ag on the surface. The average crystallite size of all samples was about 20 nm. The FESEM revealed the uniformity in size and approximately spherical shape of ZnO nanoparticles. The BET data suggest that all prepared samples are mesoporous. All prepared samples showed higher photocatalytic efficiency in the degradation of the Reactive Orange 16 (RO16) azo dye than the commercial ZnO. In addition, Ag modified ZnO powders, especially those with 1.5 and 0.75 mol% of Ag, were more efficient than the unmodified one.

Keywords: *Ag modified ZnO, nanopowders, solvothermal synthesis, photocatalysis, Reactive Orange 16*

I. Introduction

Today a great part of water pollution is caused by industrial waste waters, chemical or agricultural wastes. The large dyes consumption in industry is released into the waste water (usually at concentration between 10 and 200 mg/dm^3) [1] and this has led to a serious pollution. Nanostructured semiconducting materials present promising candidates in the field of heterogeneous photocatalysis causing a huge impact on the technology for the total degradation of various organic pollutants, including textile dyes [2].

Between many other semiconductors [3], ZnO appears to be the most promising photocatalyst and an appropriate alternative to TiO_2, because it is an inexpensive, photoactive, chemically stable, easy to prepare and non-toxic material. The great advantage is that ZnO absorbs a larger part of the solar spectrum than TiO_2. Undoped, pure ZnO was successfully applied in degradation of the following dyes: Acid Brown 14 [4], Ramazol Red [5], Basic Yellow Auramine O-A [6], Acid Red 14 [7], etc. There are only four studies [8–11] where the photodegradation of RO16 dye by ZnO was attempted under different conditions.

In photocatalysis, priority is to obtain material that can be used under natural sunlight for the wastewater purification. The modification of semiconductor photocatalysts with noble metals can improve their activity by inhibiting the electron-hole recombination [12,13], and because nanoparticles of noble metals are able to absorb visible light due to the surface plasmon resonance (SPR) [14,15]. Thus, the semiconductor band gap energy is reduced and photocatalyst can be active in the visible spectrum.

*Corresponding author: tel: +381 11 3370 477,
e-mail: *bojanasimovic@imsi.bg.ac.rs*

Azo dyes as the largest and the most important class of organic dyes are especially used for dyeing cellulose fibers. The lack of literature data related to degradation of RO16 azo dye using ZnO or modified ZnO materials, prompted us to investigate photocatalytic activity of Ag modified ZnO. RO16 dye is widely used in the textile industry and it belongs among hazardous carcinogenic pollutants. Removal of RO16 is frequently investigated as a model system using various semiconducting materials, commonly TiO_2, then composites, natural or synthetic adsorbents, etc.

Previous studies for some dyes, related to the use of Ag modified ZnO report contradictory results, in many cases the activity is enhanced [13,16–24], but in some it is inhibited [25,26]. However, there is no research dealing with degradation of RO16. The differences in their photocatalytic activity are probably associated to the: synthesis procedure, calcination temperature, nanoparticles agglomeration in dye solution, or metal content and its dispersion. For all these reasons, the investigations concerning photodegradation of RO16 using Ag/ZnO are of increasing importance.

Unlike novel solution methods, as hydrothermal and solvothermal processing, there are many physical and chemical methods for preparation of photocatalysts. Physical methods usually demand an expensive equipment and complex processing. In recent decades, the aim is the optimal energy consumption and the development of environmentally friendly materials. The main advantage of the solvothermal method is obtaining oxides in a single-step process, which eliminates the need for subsequent calcination and grinding. Another advantage is the usage of inexpensive precursors and a simple apparatus. Therefore, the solvothermal technique with its own characteristics has taken an important role in research [27]. It is still a challenge, because there are no exhaustive studies on the solvothermal synthesis that is suitable for preparation of Ag/ZnO nanoparticles of desired size, shape and properties.

The aim of this study was to obtain nanocomposite powder consisting of metallic Ag homogeneously dispersed onto surface of ZnO nanoparticles. Design of such nanocomposite should provide an increase in efficiency in the photodegradation of dye. In this work, solvothermally prepared unmodified and Ag modified ZnO nanopowders were compared with the commercial ZnO for their efficiency in the photodegradation of RO16 dye in aqueous solution, using imitated sunlight illumination. Optimization of Ag content is also presented. Ag/ZnO nanopowders obtained by this simple and low-cost method have shown a high efficiency for azo dye photodegradation and represents a promising alternative for the wastewater treatment.

II. Experimental

2.1. Solvothermal preparation

To prepare the precursor, 1.32 g of poly(vinyl pyrrolidone) (PVP - Sigma Aldrich) as surfactant was dissolved in 55 ml of ethylene glycol (EG - Carlo Erba) and then 2.64 g of solid $Zn(CH_3COO)_2 \cdot 2H_2O$ (Sigma Aldrich) was slowly added into the solution. All chemicals were of analytical grade and used without further purification. The resulting mixture was stirred, followed by the addition of 1.32 g of solid NaOH. An aliquot of 65 ml of the white mixture was treated solvothermally using a Teflon-lined stainless steel autoclave (V = 75 ml) at 120 °C for 18 h under autogenous pressure. After spontaneous cooling to room temperature, the white precipitate at the bottom of the autoclave was washed several times with distilled water and alcohol, and dried at 105 °C for 3 h. The obtained unmodified ZnO powder (0% Ag/ZnO) was white coloured as expected.

For preparation of Ag modified ZnO photocatalysts (Ag/ZnO), 1.32 g of PVP was dissolved in 55 ml of EG and then the $Zn(CH_3COO)_2 \cdot 2H_2O$ with different $AgNO_3$ (Laphoma) content (0.75, 1.5, 3 and 6 mol%) was stirred with 1.32 g NaOH. The brown precursor mixture was further treated in the same way as described above. The colour of the obtained Ag/ZnO catalysts was olive-green being slightly lighter with increasing Ag content.

2.2. Characterization of photocatalysts

The X-ray powder diffraction (XRPD) has been used for the identification of crystalline phases and calculation of crystallite size and strain. The XRPD patterns were collected over the range $25° < 2\theta < 90°$ on an Ital Structures APD2000 X-ray diffractometer using Cu$K\alpha$ radiation (λ = 1.5418 Å) with the step size of 0.1° and the counting time of 10 s/step.

The size and morphology of the prepared nanoparticles were characterized using field emission scanning electron microscopy (FESEM, Tescan Mira X3) and transmission electron microscopy (TEM, JEOL, Model 2100) equipped with an EDS attachment.

The specific surface area and the pore size distribution (PSD) of prepared ZnO specimens were analysed using the Surfer (Thermo Fisher Scientific, USA). PSD was estimated by applying BJH method [28] to the desorption branch of isotherms and mesopore surface and micropore volume were estimated using the t-plot method [29].

Micro-Raman scattering measurements were performed in the backscattering geometry by a Jobin-Yvon T64000 triple spectrometer, equipped with a confocal microscope and a nitrogen-cooled CCD detector. The Raman spectra of powders pressed into pellets were excited by VerdiTM G-Series Optically Pumped Semiconductor Laser operating at 532 ± 2 nm with output power of ~50 mW. The spectral resolution of the Raman system was ~2 cm^{-1}. All spectra were collected at room temperature in air (using 50× magnification objectives, with exposure time of 600 s) and then calibrated against the strongest Raman band of polished Si wafer (at ~520.6 cm^{-1}).

Diffuse reflectance UV-vis spectra, in the region of 200–800 nm with $BaSO_4$ as an internal standard, were

recorded employing a Shimadzu UV-2600 spectrophotometer with an integrating sphere.

2.3. Photocatalytic experiments

Photodegradation was performed using an open reactor (volume 100 ml) in a dark chamber equipped with an Osram Ultra-Vitalux 300 W lamp, which, according to the specification, produces radiation similar to the radiation of natural sunlight. The light intensity of lamp was measured using Voltcraft PL-110SM Solar Radiation Measuring Instrument and found as 300 W/m^2. The lamp was placed 35 cm away from the surface of the dye solution. Constant mixing and temperature (20 °C) of the solution was maintained during the experiment. The photodegradation of Reactive Orange 16 (RO16 Sigma Aldrich) was studied by mixing 50 ml of an aqueous solution containing dye (50 mg/dm^3) and ZnO catalyst (100 mg). The homogenous suspension left in the dark for 30 min to achieve adsorption equilibrium. Subsequently, the lamp was switched on and after every 15 min of irradiation the solution (3 ml) was sampled. The residual concentration of dye was determined using a UV-vis spectrophotometer (Shimadzu 2600) after separation of the solution by a Whatman 0.45 μm membrane filter. The absorption spectra and rate of photodegradation were observed in terms of the absorbance change at the peak maximum of the dye (λ_{max} = 492.5 nm). The commercial ZnO (MKN-ZnO-020, with a primary diameter of 20 nm and surface area of 50.72 m^2/g [30], according to the producer's specification), was treated in the same way for comparison. The selection of commercial ZnO was based on the similarity of the diameter of particles to that of prepared photocatalysts.

III. Results

3.1. Structural characterization

The XRPD patterns (Fig. 1) showed that the predominant phase in all samples is ZnO, which crystallizes in the hexagonal wurtzite structure with *P63mc* (no. 186) space group (PDF card number 80-0074). It can be seen that the diffraction peaks belonging to Ag start appearing at the 1.5% Ag/ZnO, becoming more visible in samples with 3 and 6% of Ag content. Metallic Ag crystallized in common face-centred-cubic structure (PDF card number 65-2871). No other phases, such as $Zn(OH)_2$, or from the silver-oxygen system (Ag_2O, AgO, etc), could be detected [16,20]. The main XRD peaks 111 and 200 [23] due to Ag phase increased from the 1.5 to 6% Ag/ZnO sample. The unit cell parameters and volumes, together with an average crystallite size and strain of ZnO calculated using Williamson-Hall (W-H) method [31] are shown in Table 1. There was no substantial shift of experimental peaks confirming a negligible difference in the unit cell parameters and volumes of all prepared samples. This indicates that $Zn_{1-x}Ag_xO_1$ solid solutions were not formed, but suggests that Ag was dispersed onto ZnO surface. Insignificant strain of prepared samples was probably due to the low concentration of defects meaning that the obtained structures were well ordered. This is not true for commercial sample where the manner of preparation is not known. In general, the average crystallite size of all samples was around 20 nm.

FESEM images for the samples are shown in Fig 2. The commercial ZnO (Fig. 2f) consisted of nanoparticles with a slightly elongated spherical shape. All of the obtained photocatalysts are pretty similar consisting of

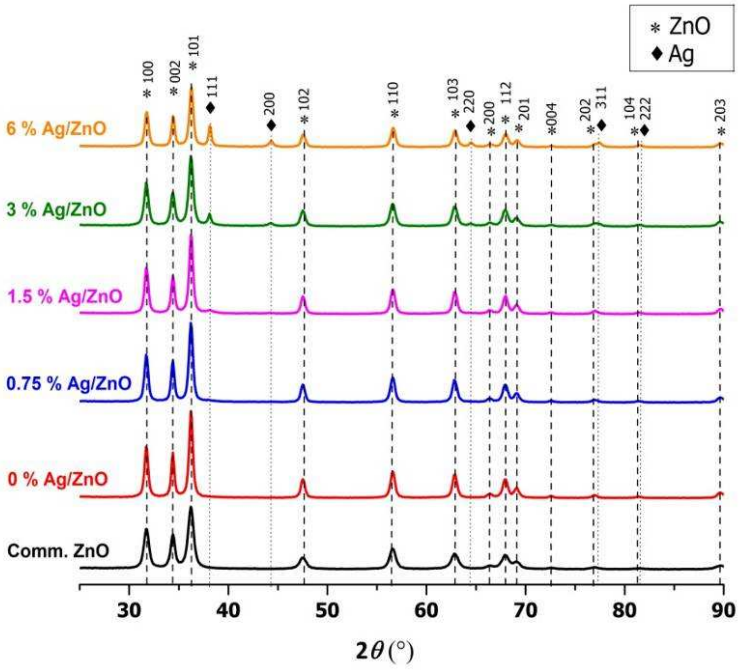

Figure 1. XRPD patterns of the commercial and synthesized ZnO nanopowders

Table 1. The summarized results of characterization: the unit cell parameters (a and c) and volumes (V), the average crystallite size (D) and strain estimated by W-H method, the band gap energy (E_g), the specific surface areas calculated by BET and t-plot method ($S_{BET} = S_{meso}$), the median pore radius (r_{med}), the reaction rate constant (k) and the corresponding correlation coefficients (R^2) of the investigated samples

Sample name	Unit cell parameters [Å] and volume [Å^3]	Williamson-Hall method D [nm]	Strain [%]	E_g [eV]	S_{BET} [m^2/g]	r_{med} [nm]	k [min^{-1}]	R^2
Commercial ZnO	a = 3.2520(1) c = 5.2178(2) V = 47.788(3)	22(1)	0.25(3)	3.15	-	-	0.0206	0.980
0% Ag/ZnO	a = 3.2533(1) c = 5.2069(2) V = 47.725(3)	21(1)	0.02(3)	3.20	29	21	0.0336	0.997
0.75% Ag/ZnO	a = 3.2536(1) c = 5.2063(2) V = 47.730(3)	21(1)	0.02(3)	3.09	24	23	0.0452	0.996
1.5% Ag/ZnO	a = 3.2518(1) c = 5.2141(2) V = 47.748(3)	22(1)	0.01(2)	3.11	30	22	0.0454	0.996
3% Ag/ZnO	a = 3.2505(1) c = 5.2097(2) V = 47.669(3)	18(1)	0.01(2)	3.12	25	19	0.0359	0.989
6% Ag/ZnO	a = 3.2511(1) c = 5.2110(2) V = 47.698(3)	21(1)	0.01(2)	3.07	43	14	0.0347	0.998

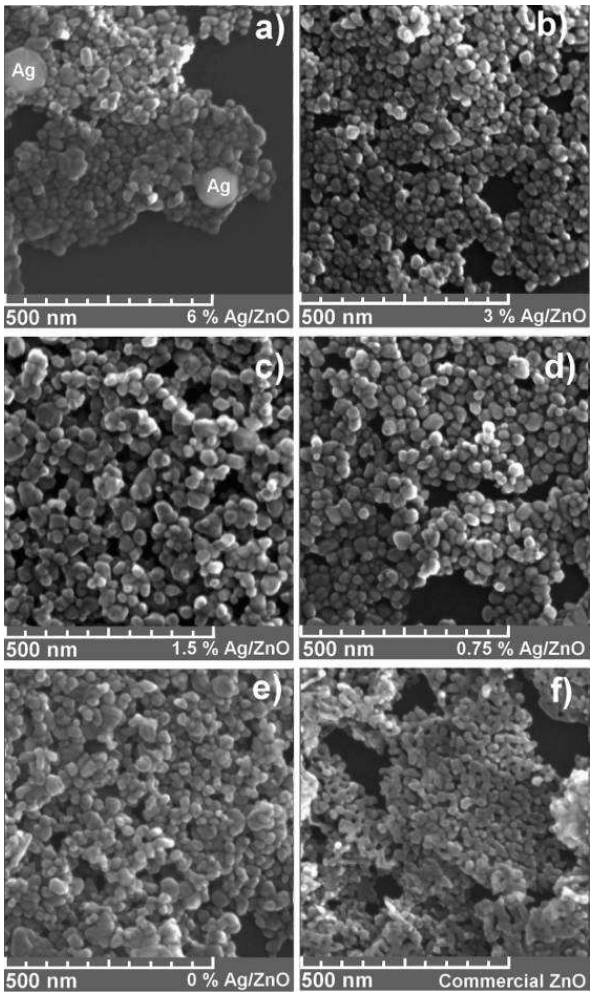

Figure 2. FESEM images of the investigated samples with the same magnification

nanoparticles with approximately spherical shape creating very soft agglomerates. The average particle size was around 25 nm for all samples. Only in the sample with 6% of Ag (Fig. 2a) one can see large particles of Ag with diameter >50 nm.

The back-scattered mode of FESEM, an imaging mode that accents atomic number contrast, confirmed that silver dispersion (arrowed) was located onto ZnO matrix (Fig. 3), simultaneously presented as nanoparticles and clusters. Figure 3 suggests that the increased Ag content leads to grouping of Ag particles. It was noticed that the samples with a lower Ag content (Figs. 3c and 3d) had a better distribution and smaller Ag particles over ZnO surface than in the case of the 3% Ag/ZnO and 6% Ag/ZnO samples; Ag particles are grouped at high Ag-content (Fig. 3a). This could cause negative effects, such as light blocked by the large Ag particles and the unequal distribution of Ag on ZnO, which result in the decrease of photocatalytic activity. Similar results were found for Ag doped TiO_2 [32,33].

From TEM images in Fig. 4 we estimated an average particle size of approximately 20 nm. Also, in HRTEM images one can see that the whole particle of ZnO has the same orientation, i.e., the whole particle is one crystallite. Thus, an excellent agreement exists between the sizes calculated from the XRPD data and the sizes determined by TEM. It is showed (Fig. 4) that the shape of nanocrystallites was irregular spherical, or, in low percent, rounded hexagonal. In addition, the larger Ag particles were confirmed in the 6% Ag/ZnO sample (Fig. 4a).

The high-resolution TEM (HRTEM) image of the 1.5% Ag/ZnO photocatlyst (Fig. 5a) showed the presence of ZnO (100) plane with the d spacing of 0.282 nm.

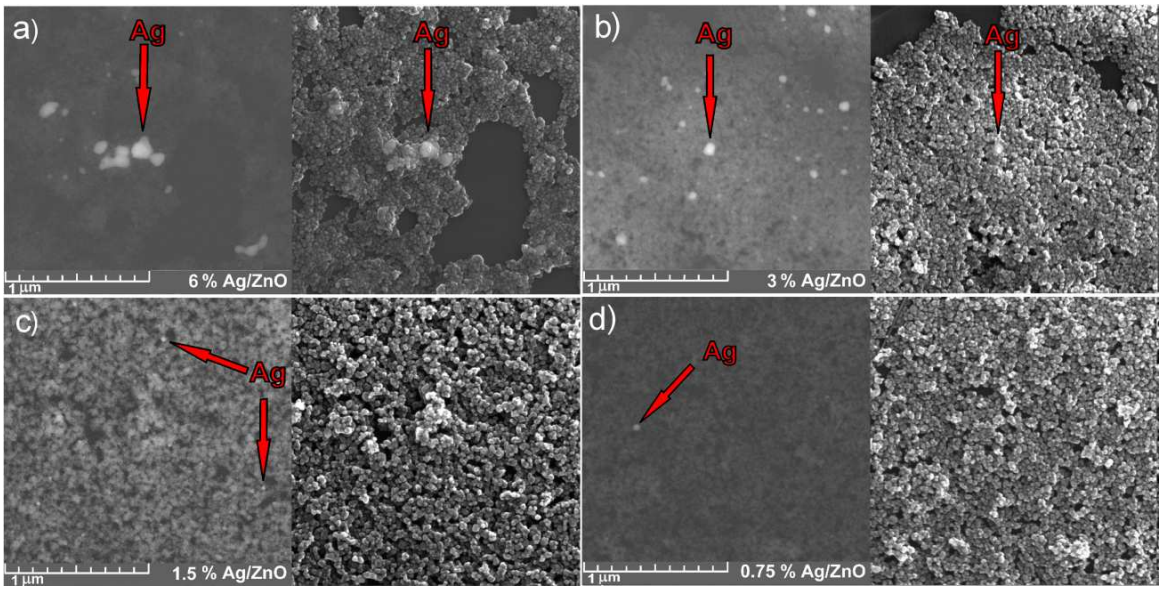

Figure 3. Simultaneously measured secondary and back-scattered electron FESEM images of: a) 6% Ag/ZnO, b) 3% Ag/ZnO, c) 1.5% Ag/ZnO and d) 0.75% Ag/ZnO

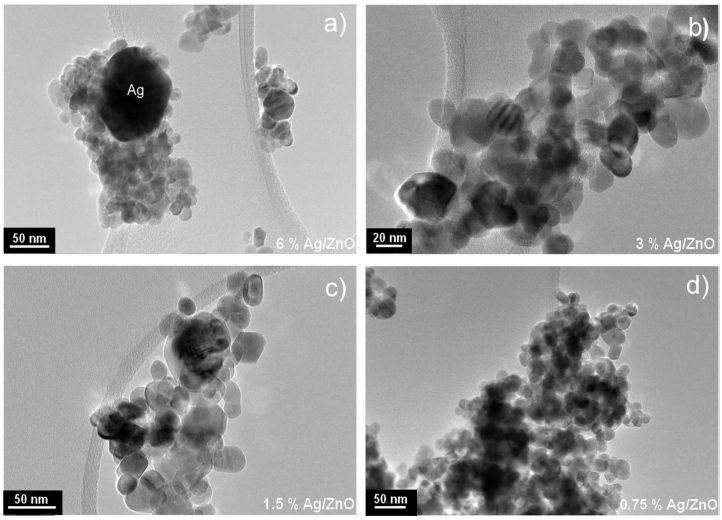

Figure 4. TEM images of: a) 6% Ag/ZnO, b) 3% Ag/ZnO, c) 1.5% Ag/ZnO and d) 0.75% Ag/ZnO

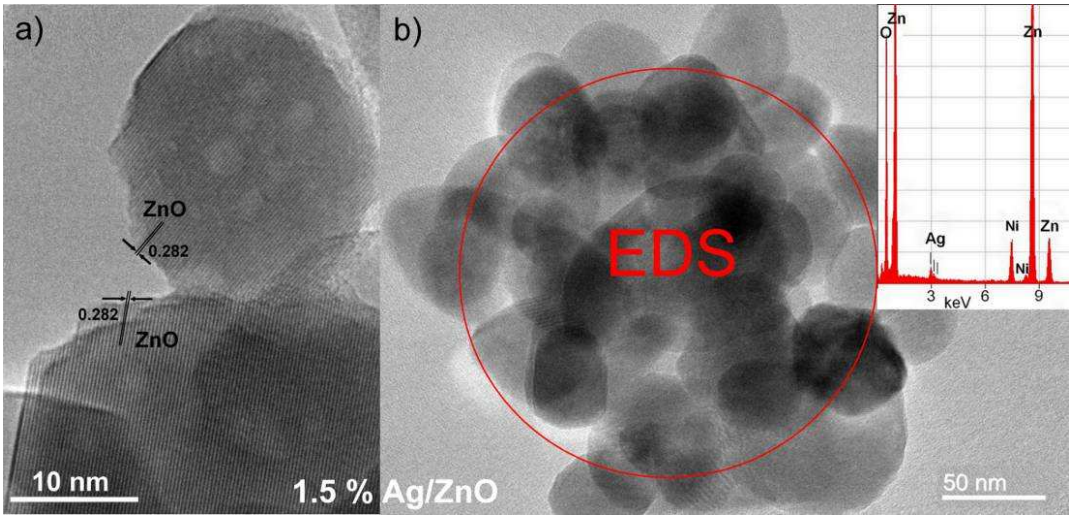

Figure 5. a) HRTEM and b) TEM images of the 1.5% Ag/ZnO sample (inset: the corresponding EDS spectrum)

The EDS analysis (Fig. 5b, inset) of group of ZnO particles (Fig. 5b) confirmed a small presence of Ag. According to XRPD data Ag did not incorporate into ZnO lattice, so it is supposed that metallic Ag is spread over ZnO surface.

3.2. Spectral analyses

UV-vis measurements

The UV-vis spectra of the samples in the diffuse reflectance mode (R) are shown in Fig. 6. The pure ZnO samples showed the highest reflectance, while Ag/ZnO samples demonstrated lower reflectance in the visible light region. The strong optical absorption at about 370 nm is characteristic of ZnO direct band gap transition [17]. Comparing with pure ZnO, all prepared Ag/ZnO samples showed a broad band in the visible region. This band is associated with the SPR peaking around 450 nm confirming the formation of metallic Ag particles. This is in accordance with the presence of stable Ag particles dispersed on the ZnO matrix [14].

The band gap values were calculated from the plot of the modified Kubelka-Munk function $(F(R)E)^2$ vs. the energy of the adsorbed light (E) [34–36] using linear fits close to the absorption edge (Fig. 7). The literature data for the optical band gap of pure ZnO show a variety of values (3.1–3.4 eV) [37], but these values were usually defined as 3.37 eV [24,25,38]. As seen in the Kubelka-Munk plots, the absorbance edge of Ag modified samples is red shifted to the longer wavelengths in the visible region, with general narrowing of band gap in the Ag/ZnO nanocomposites (Table 1). As the result, the silver modifying enhanced the visible light absorption ability of the ZnO photocatalysts. On the other hand, a remarkable change of band gap with increasing the amount of Ag, was not observed.

Raman scattering measurements

The Raman features in the spectra (Fig. 8) of the 0% Ag/ZnO and commercial ZnO powders are ascribed

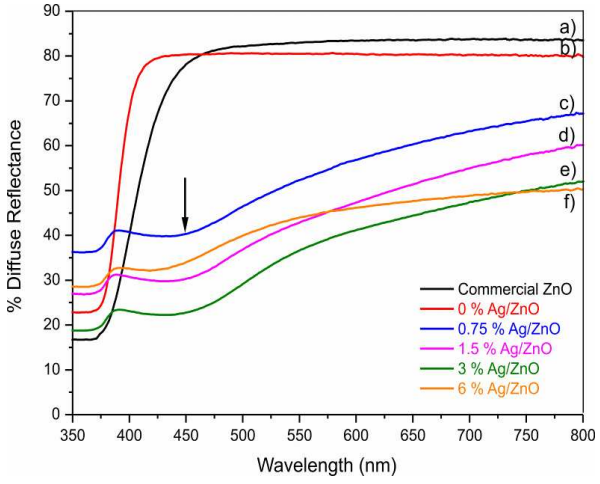

Figure 6. UV-vis diffuse reflectance spectra of: a) commercial ZnO b) 0% Ag/ZnO, c) 0.75% Ag/ZnO, d) 1.5% Ag/ZnO, e) 3% Ag/ZnO and f) 6% Ag/ZnO

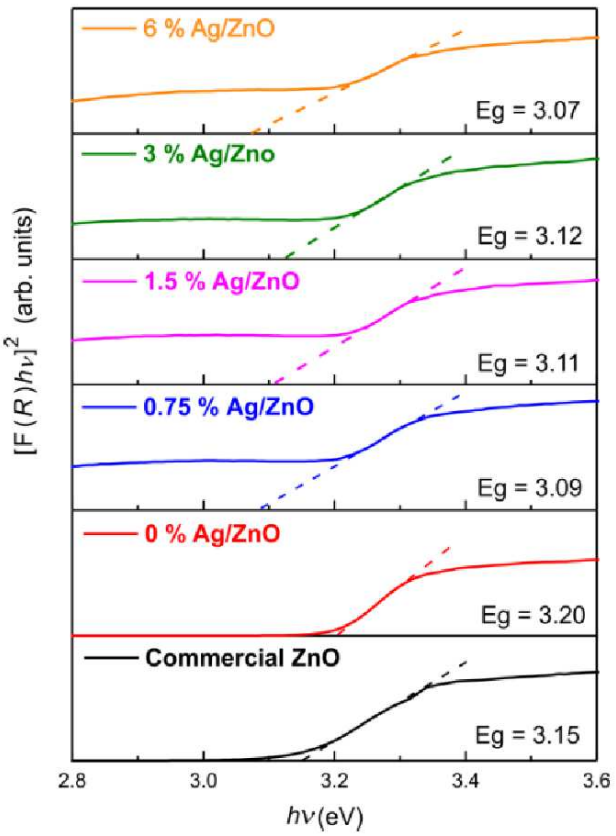

Figure 7. The plot of $(F(R)h\nu)^2$ as a function of photon energy for direct band gap transition in ZnO samples with characteristic tangent lines

to the Raman active modes of the ZnO wurtzite crystal [39]. The most pronounced features in both spectra are a narrow peak at ~98 cm^{-1} and an asymmetric peak at ~437 cm^{-1}, assigned to E_2^{low} and E_2^{high} Raman modes, respectively [39]. Red shift of about 1 cm^{-1} and broadening of these modes in comparison to the values in the bulk ZnO crystal may be a consequence of phonon confinement effect due to nanometric size of ZnO crystallites and/or lattice disorder [40]. Besides E_2 phonons, ZnO wurtzite structure is characterized by A_1 and E_1 polar phonons splitted into TO and LO phonons. In the spectra of the 0% Ag/ZnO and commercial ZnO, the peak at about 582 cm^{-1} can be ascribed to the combination of A_1(LO) and E_1(LO) modes, whereas both A_1(TO) and E_1(TO) modes are very weak and hardly detected. The most intensive second-order mode in low-wavenumber region at ~329 cm^{-1}, is ascribed to the difference $E_2^{high} - E_2^{low}$ whereas broad feature in the high-wavenumber region between 1050 and 1200 cm^{-1} contains contributions of $2A_1$(LO) and $2E_1$(LO) modes. Additionally observed features only in the spectrum of commercial ZnO: a relatively high spectrum background, lower intensity, slightly more pronounced broadening and shift of the first-order ZnO Raman modes, indicate that commercial powder is probably more disordered than unmodified ZnO powder.

E_2^{low} and E_2^{high} Raman modes of ZnO crystal struc-

ture are also observed in the spectra of Ag/ZnO samples. Besides the Raman modes ascribed to ZnO crystal, the shoulder at ~146 cm^{-1} and broad feature at ~228 cm^{-1} are the most prominent in all spectra of Ag/ZnO samples. In the Raman spectra of materials containing Ag, the feature at about 146 cm^{-1} has been usually attributed to the Ag lattice vibrational mode (phonons) [41], whereas most of the authors have attributed the features in the range between 220–240 cm^{-1} to the stretching vibrations of Ag–N and/or Ag–O bonds [42]. However, several authors have correlated mode at ~230 cm^{-1} with local vibrations of Ag atoms in the ZnO host matrix [43]. Note also that Raman scattering enhancement in the Ag modified samples can be related to the localized SPR commonly seen in the samples with Ag nanoparticles under the visible laser irradiation [44].

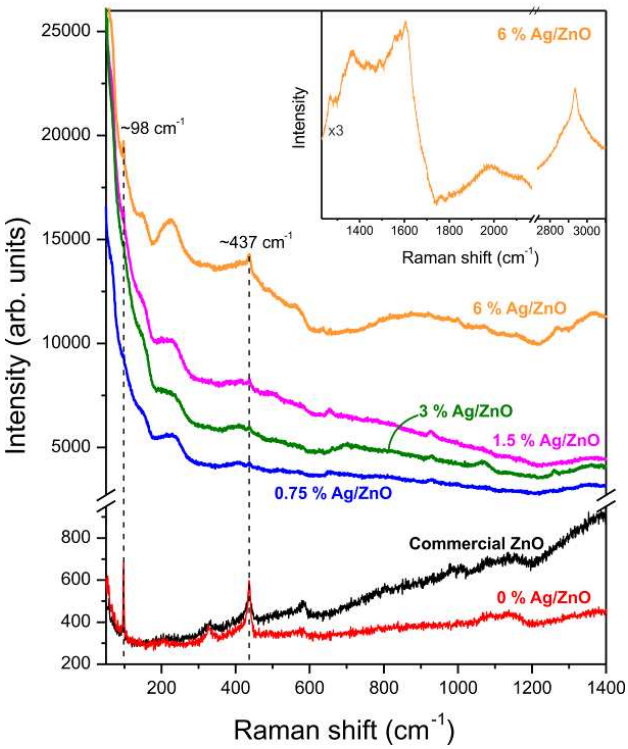

Figure 8. Raman spectra of the commercial and all synthesized ZnO powders in so-called fingerprint region (50–1400 cm^{-1}) (inset: higher frequency region (1220–3100 cm^{-1}) of Raman spectrum of 6% Ag/ZnO sample)

Several low intensity Raman features appearing in all spectra of Ag/ZnO samples can be related to the vibrational modes of organic functional groups. Most of these groups (C=O, CH_2, CH_3, $C(NO_2)$, CC, and/or COO) are an integral part of the starting substances used in the synthesis of Ag/ZnO powders. However, the lack of intensive modes characteristic for majority of starting compounds points to their decomposition during the synthesis process, with the exception of PVP. Namely, the occurrence of small peak at ~926 cm^{-1}, shoulder at ~1670 cm^{-1} and strong Raman feature with the maximum at ~2936 cm^{-1} could be a consequence of the residual traces of PVP in the synthesized ZnO samples.

3.3. *Adsorption isotherms – BET experiments*

Nitrogen adsorption isotherms for the synthesized samples, as the amount of N_2 adsorbed as function of relative pressure at −196 °C, are presented in Fig. 9a. According to the IUPAC classification [45], isotherms of the prepared ZnO samples are of type IV with a hysteresis loop which is associated with mesoporous mate-

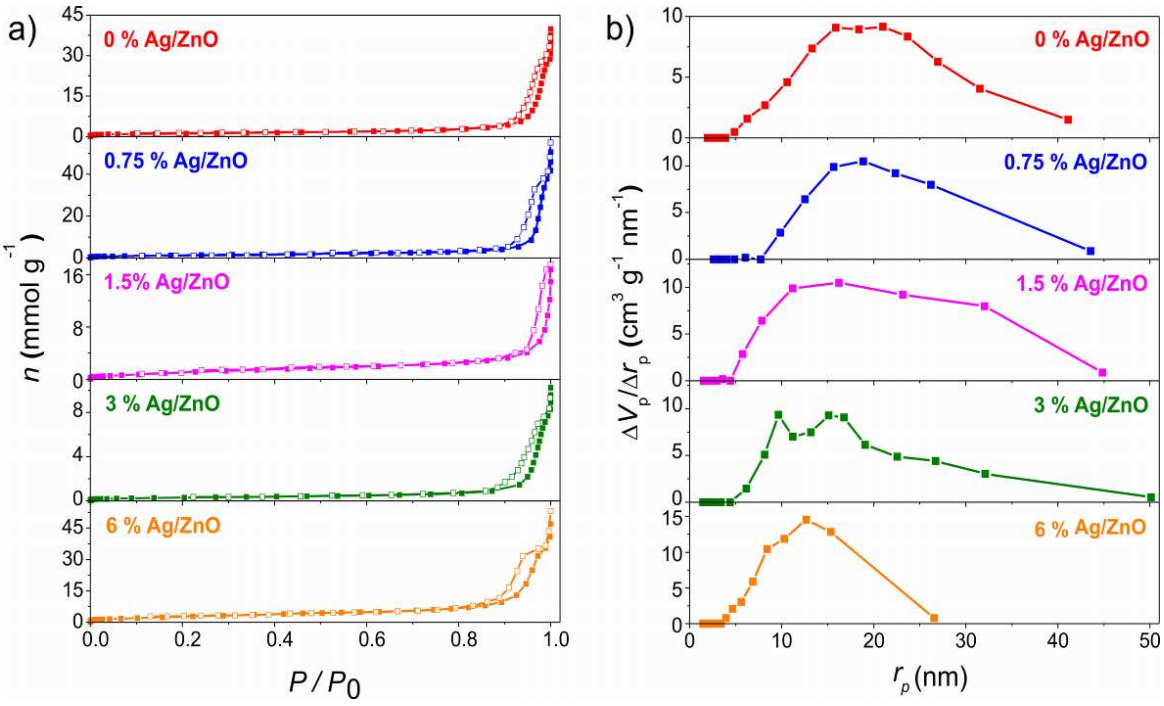

Figure 9. Nitrogen adsorption isotherms (as the amount of N_2 adsorbed as a function of relative pressure) (a) and pore size distribution (PSD) for samples (b) (solid symbols – adsorption, open symbols – desorption)

rials. In all samples, the shape of hysteresis loop is of type H3. Isotherms revealing type H3 hysteresis do not exhibit any limiting adsorption at high P/P_0, which is usually observed with non-rigid aggregates of plate-like particles giving the rise of slit-shaped pores [46].

Specific surface areas calculated by BET equation, S_{BET}, are listed in Table 1. S_{BET} values lie within 24 and 43 m^2/g. A systematic change of specific surface, with an increase of the Ag amount, was not observed. Samples with Ag percent between 0.75–3% had similar specific surface as unmodified ZnO. However, addition of 6% of Ag increased the overall specific surface to 43 m^2/g.

PSD of the samples (Fig. 9b) shows that samples are mesoporous with the pore radius between 2 and 50 nm. The median pore radius (Table 1) slightly decreased with an increase of Ag content. This shows that the increased Ag content causes the reduction of the pore size available for adsorption of dye molecule which could be related to the decrease of photocatalytic efficiency.

The *t*-plot is obtained on the basis of the standard nitrogen adsorption isotherm (Fig. 10). The straight line in the medium *t*-plot region provides a mesoporous surface area including the contribution of external surface, S_{meso}, determined by its slope, and the micropore volume, V_{mic}, is given by the intercept. S_{meso} values were equal as S_{BET} *t*-plot analysis confirming that all samples were completely mesoporous.

3.4. Photocatalytic decolourisation of RO16 dye

The power of the samples during the dark adsorption and photocatalytic decolourisation of RO16, is shown in Fig. 11. The same trend between dye adsorption and degradation was observed for all samples. It was also experimentally verified that there was no photodegradation of dye in UV-vis light in the absence of a catalyst. As shown, all synthesized samples had a higher adsorption efficiency and photocatalytic activity than the commercial ZnO. The order of decreasing activity was 1.5% Ag/ZnO ≈ 0.75% Ag/ZnO > 3% Ag/ZnO > 6% Ag/ZnO > 0% Ag/ZnO > commercial ZnO. The lower adsorption efficiency in the dark of the commercial ZnO could be tentatively ascribed to the slightly sintered grains (Fig. 2f) and the existence of significant strain in this case (Table 2).

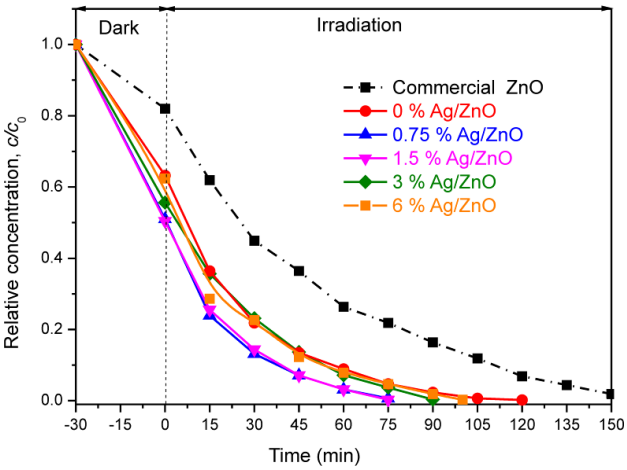

Figure 11. The rate of photodegradation of RO16 in aqueous unmodified and Ag modified ZnO suspensions (experimental conditions: RO16 50 mg/dm³, pH = 6.7, catalyst suspension 2 g/dm³)

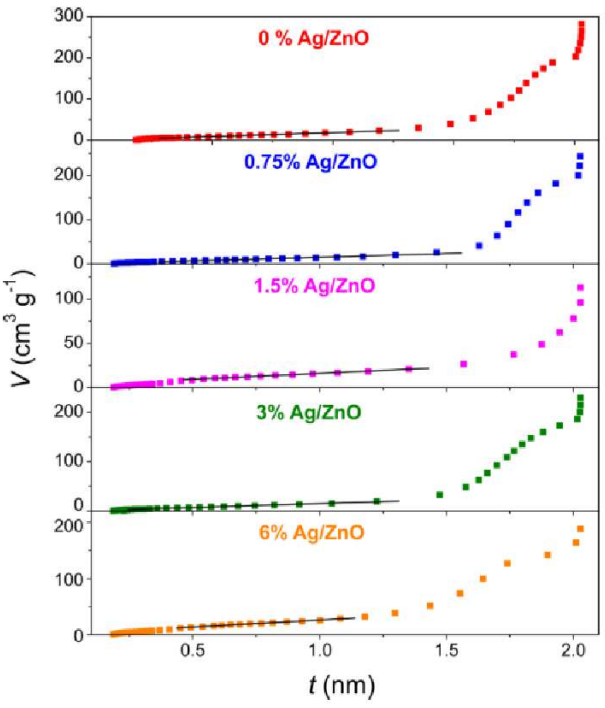

Figure 10. *t*-plots for nitrogen adsorption isotherm of the prepared samples

RO16 is a large molecule (molecular weight 617.54), hence its complete decomposition is complex and passes through many intermediate states [47]. The kinetics of photodegradation rate for most of dyes can be well described using Langmuir-Hinshelwood kinetic model [23,48–50]. The kinetics parameters (reaction rate constants and correlation coefficients) for the photocatalytic removal of RO16 were calculated by the fitting assuming pseudo-first kinetic order of the reaction, $\ln(c_0/c) = kt$, where c_0 is the initial concentration of the dye (mg/dm³), c is the concentration (mg/dm³) at any time, t (min) and k is the reaction rate constant (min^{-1}). Generally the pseudo-first kinetic order is proper for the concentration up to 60 mg/dm³ and many studies were well fitted by this model [51,52]. In our case, the logarithmic plots of concentration data gave a straight line (Fig. 12). The correlation coefficients (R^2) for the fitted line were in the range from 0.980 to 0.998 (Table 1). This confirmed the pseudo-first order model to describe the kinetics of RO16 degradation. The same kinetic model was used by Roselin for photodegradation of RO16 by pure ZnO [10].

Our results proved that all Ag modified ZnO powders were more efficient than the unmodified one, while the photodegradation rate decreased at higher Ag con-

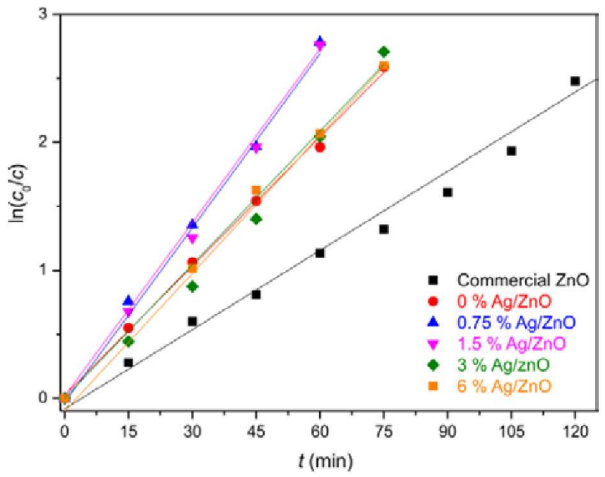

Figure 12. Plots of $\ln(c_0/c)$ versus reaction time for the degradation of the aqueous solution of RO16 dye (50 mg/dm^3) with content of the investigated samples 2 g/dm^3

tent. This is probably due to the presence of Ag clusters decreasing surface availability on the particles for dye adsorption and light absorption. For example, the samples containing 1.5 and 0.75 mol% of Ag reached the maximum photocatalytic activity with the rate constants (k) of 0.0454 and 0.0452 min^{-1}, respectively (Table 1). Thus, the best prepared photocatalysts completely decolorized RO16, around 2 times faster than the commercial ZnO, probably due to the better Ag distribution over ZnO nanoparticles for these two samples (Fig. 3).

IV. Discussion

The aim of this work was to investigate the influence of Ag on the structural, microstructural, spectral and photocatalytic properties of Ag/ZnO nanopowders that have been synthesized by using solvothermal method at 120 °C for 18 h.

XRPD, FESEM, TEM/EDS, UV-vis and Raman measurements confirmed the presence of ZnO nanocrystallites and metallic Ag. These analyses showed no significant difference in the crystallite and particle size, as well as in morphology between the obtained samples. The average crystallite size ~20 nm, the average particle size ~25 nm and approximately spherical shape of the nanoparticles were characteristic for all obtained specimens. Here, PVP, mutually with EG, played an important role in controlling the size and shape of the ZnO particles during the synthesis, causing the uniformity in size and morphology of the particles. The application of PVP as a surfactant was important for small crystallite and particle sizes and thus the use of this polymer is strongly recommended for the future research [53,11].

According to some previous reports, Ag can be incorporated into ZnO lattice, either as a substituent for Zn^{2+} or as an interstitial atom [54], but mostly onto ZnO surface [17,21–25,55]. It does not seem probable that Ag incorporates into ZnO because of a high difference in ionic radii between Zn^{2+} (0.72 Å) and Ag^{+} (1.22 Å). Therefore, Ag particles prefer to gather on the ZnO surface [26]. Considering our XRPD results, it could be concluded that Ag atoms were not incorporated into the ZnO lattice, or if so, then it was below the limits of detection. Hence, Ag nanoparticles are generally located on the ZnO surface that has been proved by FESEM, TEM and UV-vis techniques.

The phase purity of the samples was confirmed by XRPD analysis, although the residual traces of PVP were detected by Raman analysis in Ag/ZnO samples. Note that Raman spectroscopy provides a higher sensitivity to research the surface of nanomaterials especially in the presence of Ag nanoparticles [44], leading to the appearance of Raman features originated from the sample components with extremely low concentration. However, from our previous work [11], it was concluded that the presence of these traces impurities in prepared ZnO samples had a minor or no influence on their photocatalytic activity. It should be mentioned that XRPD and Raman analysis indicate that the commercial ZnO is probably more disordered than prepared ZnO samples which resulted in the decrease of photocatalytic activity of the commercial ZnO.

The differences between certain samples were established after UV-vis, BET and photocatalytic measurements. All ZnO samples showed good optical absorption behaviour. Pure ZnO powders showed light UV absorption while the modification with Ag enhanced the visible light absorption ability due to the SPR and thus increased the photocatalytic activity [13,14]. On the other hand, a systematic change of photodegradation of RO16 (Fig. 13) depending on the band gap (Table 1), with increasing Ag amount, was not observed. It can be concluded that Ag content was not the primary factor in photocatalytic efficiency and with a very low Ag content one can achieve the desired photocatalytic effect.

Some previous studies [17,20,26] suggested that Ag traps electrons, reduces the recombination of photogenerated electrons (e^-) and holes (h^+) and prolongs the lifetime of the e^-/h^+ pairs. The upgrading of photocat-

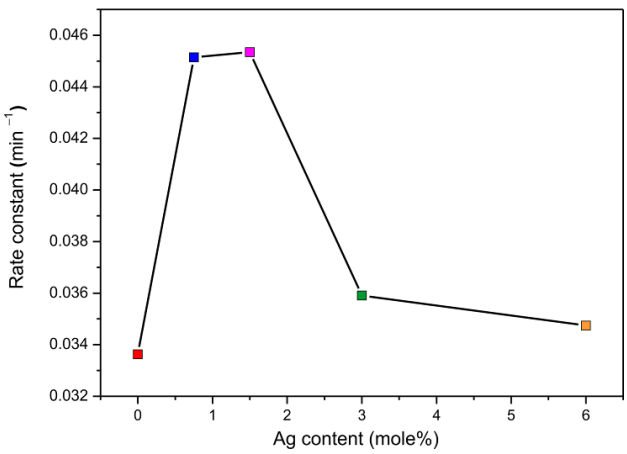

Figure 13. Rate constant (k) of RO16 degradation using ZnO and Ag/ZnO with various Ag contents

alytic efficiency by Ag nanoparticles is probably caused by equalization of the Fermi levels of the ZnO and Ag that makes the electrons transfer from the semiconductor to the silver. Then, the obtained e^-/h^+ pairs react with O_2 and OH^- producing a strong oxidant for degradation of dyes.

The photodegradation rate increases as Ag content is increased up to the 1.5 mol% of Ag and then decreases with further increase of Ag content in the Ag/ZnO samples (Fig. 13). Since the sample 0.75% Ag/ZnO had a very similar activity as the 1.5% Ag/ZnO it should be recommended for the future research from the economical aspect. The optimal amount of metal can become the center for trapping electrons, while redundant amount of metal can become the center for recombining electron-hole pairs [12,56]. The significant decrease in the photodegradation with 3% and 6% Ag/ZnO can also be ascribed to the reduced amount of dispersed surface particles available for degradation probably due to the cluster formation with increased addition of Ag onto ZnO surface. With the high Ag content, the size of the Ag clusters became too large for blocking the light to reach on the ZnO surface and occupy the active sites for the desired photocatalytic reactions [32]. Although 6% Ag/ZnO sample possesses larger surface area and slightly lower band gap value than other Ag/ZnO samples, it showed around 30 minutes slower decolourisation of RO16 comparing to the best prepared photocatalysts. This is probably due to the presence of larger Ag particles.

The obtained results clearly indicate that there is a proper content and critical particle size of Ag for the improvement of photocatalytic efficiency of ZnO [12,54,56]. Similar behaviour is observed in previous studies, but with the optimum Ag content of around 1% for Brilliant blue [22], 5% for Methyl Orange [17] and 6% of Ag for Rhodamine B dye [56].

Generally, photocatalytic properties of ZnO-based materials usually depend on the crystallinity and crystallite size, phase composition, particle size, morphology and pore sizes, surface area, band gap energy, availability of active sites, number and the nature of trapped sites, as well as on adsorption/desorption characteristics [57]. Among all the samples, the 1.5% and 0.75% Ag/ZnO have performed the highest efficiency in degradation of RO16. This could not be related to the often cited properties as preferable in photocatalysis, such as small particle size and large specific area. In fact, neither their crystallites were the smallest, nor the specific surface area of these samples was the largest nor their band gap was the lowest (Table 1). In this work, well distribution of Ag nanoparticles seems to be the crucial factor for the highest photocatalytic efficiency rather than the crystallite and particle size or surface area that has been mentioned previously [57]. Besides, the improved efficiency in photodegradation of the large molecule of RO16 (with the longest dimension estimated as 2.3 nm) can also be caused by an increase of median pore radius with the decrease of Ag content in the Ag modified samples. For example, the ZnO with 6% of Ag had the lowest median pore radius and lower photocatalytic activity than the best prepared photocatalysts (1.5 and 0.75% Ag/ZnO) with the highest median pore radius.

It is hard to compare the individual studies of photocatalytic activity, because they are performed under quite different conditions such as irradiation source, solution concentration, catalyst content, pH solution, etc. Some of them use very aggressive conditions, like powerful light sources and/or extremely short distances away from the dye solution. Nevertheless, the rate constants are often in the same order of magnitude as our results [10,24]. Studies that use quite similar conditions as ours for the degradation of RO16 by other photocatalysts are scarce. The pseudo-first order rate constants for the 1.5% Ag/ZnO and 0.75% Ag/ZnO are slightly higher than the published results on photodegradation of RO16 by commercial Degussa Aeroxide TiO_2 P25 [49], where RO16 was irradiated under the most similar conditions as in this study.

Some previous studies dealing with Ag/ZnO nanocatalysts reported contradictory results. For many azo dyes they showed the enhancement of photocatalytic activity, while for some others act as inhibitor compared to the unmodified ZnO [25,26]. Besides already mentioned reasons for their different activity, molecular structure of dyes should also be taken into account. Above all, in order to provide some deeper insight into this behaviour of Ag/ZnO it is necessary to analyze several azo dyes under the same conditions. For these reasons, photodegradation of various dyes using 0.75% Ag/ZnO is strongly recommended for further investigations. It could help to resolve above mentioned opposite results for other dyes.

V. Conclusions

In this work, the unmodified and Ag modified mesoporous ZnO nanopowders have been successfully synthesized through a simple solvothermal method. The results showed that the crystallite and particle sizes were very similar, and around 20 nm for all prepared samples. The Ag modification on the ZnO nanocrystals significantly improved its photocatalytic degradation of RO16 dye. The removal of RO16 dye followed the pseudo-first kinetic order according to the Langmuir-Hinshelwood model. The samples containing 1.5 and 0.75 mol% of Ag, demonstrated the best photocatalytic degradation of RO16 textile dye. These photocatalysts completely decolorized RO16 dye, around 2 times faster than the commercial ZnO. According to FESEM, this is probably due to the small and well distributed Ag nanograins over ZnO nanoparticles in the case of these two samples. The specimen containing 0.75 mol% of Ag had a negligibly lower photoactivity than the 1.5% Ag/ZnO sample, and it is recommended for further research in terms of economy. In summary, the photocatalytic activity of the prepared ZnO materials does not depend much on

surface area, but it depends on the median pore radius, band gap and mainly on distribution of Ag. Due to all these reasons, the photocatalytic degradation of textile effluent assisted with Ag modified ZnO materials might be an efficient method and environmentally friendly for water treatment.

Acknowledgements: This work was financially supported by the Serbian Ministry of Education, Science and Technological Development, Project No. III45007. The support of the bilateral cooperation with Slovenia is also gratefully acknowledged (Project No. 451-03-3095/2014-09/32). The TEM work was conducted in the Centre for Electron Microscopy and Microanalysis (CEMM) at Jožef Stefan Institute, Ljubljana (Slovenia).

References

1. K.H. Gonawala, M.J. Mehta, "Removal of color from different dye wastewater by using ferric oxide as an adsorbent", *Int. J. Eng. Res. Appl.*, **4** (2014) 102–109.
2. R. Andreozzi, V. Caprio, A. Insola, R. Marotta, "Advanced oxidation processes (AOP) for water purification and recovery", *Catal. Today*, **53** (1999) 51–59.
3. A.B. Djurišić, Y.H. Leung, A.M.C. Ng, "Strategies for improving the efficiency of semiconductor metal oxide photocatalysis", *Mater. Horiz.*, **1** (2014) 400–410.
4. S. Sakthivel, B. Neppolian, M.V. Shankar, B. Arabindoo, M. Palanichamy, V. Murugesan, "Solar photocatalytic degradation of azo dye: Comparison of photocatalytic efficiency of ZnO and TiO_2", *Sol. Energy Mater. Sol. Cells*, **77** (2003) 65–82.
5. A. Akyol, H.C. Yatmaz, M. Bayramoglu, "Photocatalytic decolorization of Remazol Red RR in aqueous ZnO suspensions", *Appl. Catal. B*, **54** (2004) 19–24.
6. A. Pandurangam, P. Kamala, S. Uma, M. Palanichamy, V. Murugesan, "Degradation of basic yellow auramine O-A textile dye by semiconductor photocatalysis", *Indian J. Chem. Technol.*, **8** (2001) 496–499.
7. N. Daneshvar, D. Salari, A.R. Khataee, "Photocatalytic degradation of azo dye acid red 14 in water: investigation of the effect of operational parameters", *J. Photochem. Photobiol. A*, **157** (2003) 111–116.
8. R.S. Dhodapkar, V. Chaturvedi, N.R. Neti, S.N. Kaul, "Heterogenous solar photocatalysis of two commercial reactive azo dyes", *Ann. Chim.*, **93** (2003) 739–744.
9. E. Yassıtepe, H.C. Yatmaz, C. Ozturk, K. Ozturk, C. Duran, "Photocatalytic efficiency of ZnO plates in degradation of azo dye solutions", *J. Photochem. Photobiol. A*, **198** (2008) 1–6.
10. L.S. Roselin, R. Selvin, "Photocatalytic degradation of Reactive Orange 16 dye in a ZnO coated thin film flow photoreactor", *Sci. Adv. Mater.*, **3** (2011) 251–258.
11. B. Simović, A. Golubović, I. Veljković, D. Poleti, J. Zdravković, D. Mijin, A. Bjelajac, "Hydro- and solvothermally-prepared ZnO and its catalytic effect on the photodegradation of Reactive Orange 16 dye", *J. Serb. Chem. Soc.*, **79** (2014) 1433–1443.
12. J. Liqiang, W. Dejun, W. Baiqia, L. Shudan, X. Baifu, F. Honggang, S. Jiazhong, "Effects of noble metal modification on surface oxygen composition, charge separation and photocatalytic activity of ZnO nanoparticles", *J. Mol. Catal. A: Chem.*, **244** (2006) 193–200.
13. B. Subash, B. Krishnakumar, R. Velmurugan, M. Swaminathan, M. Shanthi, "Synthesis of Ce co-doped Ag-ZnO photocatalyst with excellent performance for NBB dye degradation under natural sunlight illumination", *Catal. Sci. Technol.*, **2** (2012) 2319–2326.
14. S. Arooj, S. Nazir, A. Nadhman, N. Ahmad, B. Muhammad, I. Ahmad, K. Mazhar, R. Abbasi, "Novel ZnO:Ag nanocomposites induce significant oxidative stress in human fibroblast malignant melanoma (Ht144) cells", *Beilstein J. Nanotechnol.*, **6** (2015) 570–582.
15. E.J. Guidelli, O. Baffa, D.R. Clarke, "Enhanced UV emission from silver/ZnO and gold/ZnO core-shell nanoparticles: Photoluminescence, radioluminescence, and optically stimulated luminescence", *Sci. Rep.*, **5** (2015) 14004.
16. J. Zhi-gang, P. Kuan-kuan, L. Yan-hua, Z. Rong-sun, "Preparation and photocatalytic performance of porous ZnO microrods loaded with Ag", *Trans. Nonferrous Met. Soc. China*, **22** (2012) 873–878.
17. Y. Zheng, L. Zheng, Y. Zhan, X. Lin, Q. Zheng, K. Wei, "Ag/ZnO heterostructure nanocrystals: Synthesis, characterization, and photocatalysis", *Inorg. Chem.*, **46** (2007) 6980–6986.
18. G. Zhou, J. Deng, "Preparation and photocatalytic performance of Ag/ZnO nano-composites", *Mater. Sci. Semicond. Process.*, **10** (2007) 90–96.
19. G. Bandekar, N.S. Rajurkar, I.S. Mulla, U.P. Mulik, D.P. Amalnerkar, P.V. Adhyapak, "Synthesis, characterization and photocatalytic activity of PVP stabilized ZnO and modified ZnO nanostructures", *Appl. Nanosci.*, **4** (2014) 199–208.
20. M.J. Height, S.E. Pratsinis, O. Mekasuwandumrong, P. Praserthdam, "Ag-ZnO catalysts for UV-photodegradation of methylene blue", *Appl. Catal. B*, **63** (2006) 305–312.
21. Z. Zhang, Y. Li, K. Li, K. Chen, Y. Yang, X. Liu, H. Jia, B. Xu, "Growth and characterization of flower-like Ag/ZnO heterostructure composites with enhanced photocatalytic performance", *J. Mater. Sci.*, **49** (2014) 2347–2354.
22. T. Parvin, N. Keerthiraj, I. A. Ibrahim, S. Phanichphant, K. Byrappa, "Photocatalytic degradation of municipal wastewater and brilliant blue dye using hydrothermally synthesized surface-modified silver-doped ZnO designer particles", *Int. J. Photoenergy*, **2012** (2012) 1–8.
23. D. Lin, H. Wu, R. Zhang, W. Pan, "Enhanced photocatalysis of electrospun Ag-ZnO heterostructured nanofibers", *Chem. Mater.*, **21** (2009) 3479–3484.
24. Y. Dong, C. Feng, P. Jiang, G.Wang, K. Li, H. Miao, "Simple one-pot synthesis of ZnO/Ag heterostructures and the application in visiblelight-responsive photocatalysis", *RSC Adv.*, **4** (2014) 7340–7346.
25. C. Karunakaran, V. Rajeswari, P. Gomathisankar, "Antibacterial and photocatalytic activities of sonochemically prepared ZnO and Ag-ZnO", *J. Alloys Compd.*, **508** (2010) 587–591.
26. R. Georgekutty, M.K. Seery, S.C. Pillai, "A highly efficient Ag-ZnO photocatalyst: Synthesis, properties, and mechanism", *J. Phys. Chem. C*, **112** (2008) 13563–13570.
27. K. Byrappa, T. Adschiri, "Hydrothermal technology for nanotechnology", *Prog. Cryst. Growth Charact. Mater.*, **53** (2007) 117–166.
28. E.P. Barret, L.G. Joyner, P.P. Halenda, "The determination of pore volume and area distributions in porous substances. I. Computations from nitrogen isotherms", *J. Am. Chem.*

Soc., **73** (1951) 373–380.
29. B.C. Lippens, B.G. Linsen, J.H. de Boer, "Studies on pore systems in catalysts: V. The t method", *J. Catalysis*, **3** (1964) 32–37.
30. W. Wu, G. Ichihara, N. Hashimoto, Y. Hasegawa, Y. Hayashi, S. Tada-Oikawa, Y. Suzuki, J. Chang, M. Kato, C.N. D'Alessandro-Gabazza, E.C. Gabazza, S. Ichihara, "Synergistic effect of bolus exposure to zinc oxide nanoparticles on Bleomycin-induced secretion of Pro-Fibrotic Cytokines without lasting fibrotic changes in Murine Lungs", *Int. J. Mol. Sci.*, **16** (2015) 660–676.
31. V.D. Mote, Y. Purushotham, B.N. Dole, "Williamson-Hall analysis in estimation of lattice strain in nanometer-sized ZnO particles", *J. Theor. Appl. Phys.*, **6** (2012) 1–8.
32. M.A. Behnajady, N. Modirshahla, M. Shokri, B. Rad, "Enhancement of photocatalytic activity of TiO_2 nanoparticles by silver doping: photodeposition versus liquid impregnation methods", *Global Nest. J.*, **10** (2008) 1–7.
33. T.D. Pham, B.K. Lee, "Feasibility of silver doped TiO_2/glass fiber photocatalyst under visible irradiation as an indoor air Germicide", *Int. J. Environ. Res. Public Health*, **11** (2014) 3271–3288.
34. P. Kubelka, F. Munk, "Ein Beitrag zur Optik der Farbanstriche", *Z. Tech. Phys.*, **12** (1931), 593–601.
35. P. Kubelka, "New contributions to the optics of intensely light-scattering materials. Part I", *J. Opt. Soc. Am.*, **38** (1948) 448–457.
36. M.P. Fuller, P.R. Griffiths, "Diffuse reflectance measurements by infrared Fourier transform spectrometry", *Anal. Chem.*, **50** (1978) 1906–1910.
37. K.G. Chandrappa, T.V. Venkatesha, "Electrochemical synthesis and photocatalytic property of zinc oxide nanoparticles", *Nano-Micro Lett.*, **4** (2012) 14–24.
38. C. Wang, E. Shen, E. Wang, L. Gao, Z. Kang, C. Tian, Y. Lan, C. Zhang, "Controllable synthesis of ZnO nanocrystals via a surfactant-assisted alcohol thermal process at a low temperature", *Mater. Lett.*, 59 (2005) 2867–2871.
39. R. Cusco, E. Alarcon-Llado, J. Ibanez, L. Artus, J. Jimenez, B. Wang, M.J. Callahan, "Temperature dependence of Raman scattering in ZnO", *Phys. Rev. B*, **75** (2007) 165202.
40. M. Šćepanović, M. Grujić-Brojčin, K. Vojisavljević, S. Bernik, T. Srećković, "Raman study of structural disorder in ZnO nanopowders", *J. Raman Spectrosc.*, **41** (2010) 914–921.
41. I. Martina, R. Wiesinger, D. Jembrih-Simbürger, M. Schreiner, "Micro-Raman characterisation of silver corrosion products:instrumental set up and reference database", *e-Preserv.Sci.*, **9** (2012) 1–8.
42. A.J. Kora, J. Arunachalam, "Green fabrication of silver nanoparticles by gum tragacanth (Astragalus gummifer): A dual functional reductant and stabilizer", *J. Nanomater.*, **2012** (2012) 1–8.
43. W.J. Li, C.Y. Kong, H.B. Ruan, G.P. Qin, G.J. Huang, T.Y. Yang, W.W. Liang, Y.H. Zhao, X.D. Meng, P. Yu, Y.T. Cui, L. Fang, "Electrical properties and Raman scattering investigation of Ag doped ZnO thin films", *Solid State Commun.*, **152** (2012) 147–150.
44. K. Rajan, I. Roppolo, A. Chiappone, S. Bocchini, D. Perrone, A. Chiolerio, "Silver nanoparticle ink technology: state of the art", *Nanotechnol. Sci. Appl.*, **9** (2016) 1–13.
45. K.S.W. Sing, D.H. Everett, R.A.W. Haul, L. Moscou, R.A. Pierotti, J. Rouquerol, "Reporting physisorption data for gas/solid systems with special reference to the determination of surface area and porosity", *Pure Appl. Chem.*, **57** (1985) 603–619.
46. S. Lowell, J.E. Shields, M.A. Thomas, M. Thommes, *Charactrization of Porous Solids and Powders: Surface Area, Pore Size and Density*, Ed. Kluwer Academic Publishers, Dordrecht Netherlands, p. 44, 2004.
47. S. Bilgi, C. Demir, "Identification of photooxidation degradation products of C.I. Reactive Orange 16 dye by gas chromatographye mass spectrometry", *Dyes Pigm.*, **66** (2005) 69–76.
48. H.C. Yatmaz, A. Akyol, M. Bayramoglu, "Kinetics of the photocatalytic decolorization of an azo reactive dye in aqueous ZnO suspensions", *Ind. Eng. Chem. Res.*, **43** (2004) 6035–6039.
49. D. Mijin, M. Radulović, D. Zlatić, P. Jovančić, "Photocatalytic degradation of textile dye C.I. reactive orange 16 in TiO_2 water suspension by simulated solar light", *Chem. Ind. Chem. Eng. Q.*, **13** (2007) 179–185.
50. S.M. Lam, J.C. Sin, A.Z. Abdullah, A.R. Mohamed, "Degradation of wastewaters containing organic dyes photocatalysed by zinc oxide: A review", *Desalin. Water Treat.*, **41** (2012) 131–169.
51. K.K. Ioannis, A.A. Triantafyllos, "TiO_2-assisted photocatalytic degradation of azo dyes in aqueous solution: kinetic and mechanistic investigations: A review", *Appl. Catal. B*, **49** (2004) 1–14.
52. C.Y. Chen, "Photocatalytic degradation of azo dye Reactive Orange 16 by TiO_2", *Water Air Soil Pollut.*, **202** (2009) 335–342.
53. T. Thirugnanam, "Effect of polymers (PEG and PVP) on sol-gel synthesis of microsized zinc oxide", *J. Nanomater.*, **2013** (2013) 1–7.
54. Ö.A. Yıldırım, H.E. Unalan, C. Durucan, "Highly efficient room temperature synthesis of silver-doped zinc oxide (ZnO:Ag) nanoparticles: Structural, optical, and photocatalytic properties", *J. Am. Ceram. Soc.*, **96** (2013) 766–773.
55. C. Chen, Y. Zheng, Y. Zhan, X. Lin, Q. Zheng, K. Wei, "Enhanced Raman scattering and photocatalytic activity of Ag/ZnO heterojunction nanocrystals", *Dalton Trans.*, **40** (2011) 9566–9570.
56. Y. Zhang, J. Mu, "One-pot synthesis, photoluminescence, and photocatalysis of Ag/ZnO composites", *J. Colloid Interface Sci.*, **309** (2007) 478–484.
57. K.M. Lee, C.W. Lai, K.S. Ngai, J.C. Juan, "Recent developments of zinc oxide based photocatalyst in water treatment technology: A review", *Water Res.*, **88** (2016) 428–448.